CONF-9505264--22

UCRL-JC-121180
PREPRINT

Plasma Electrode Pockels Cell for ICF Lasers

M. A. Rhodes
C. D. Boley
A. G. Tarditi
B. S. Bauer

This paper was prepared for submittal to the
1st Annual International Conference on Lasers for
Application to Inertial Confinement Fusion
Monterey, CA
May 30 - June 2, 1995

July 7, 1995

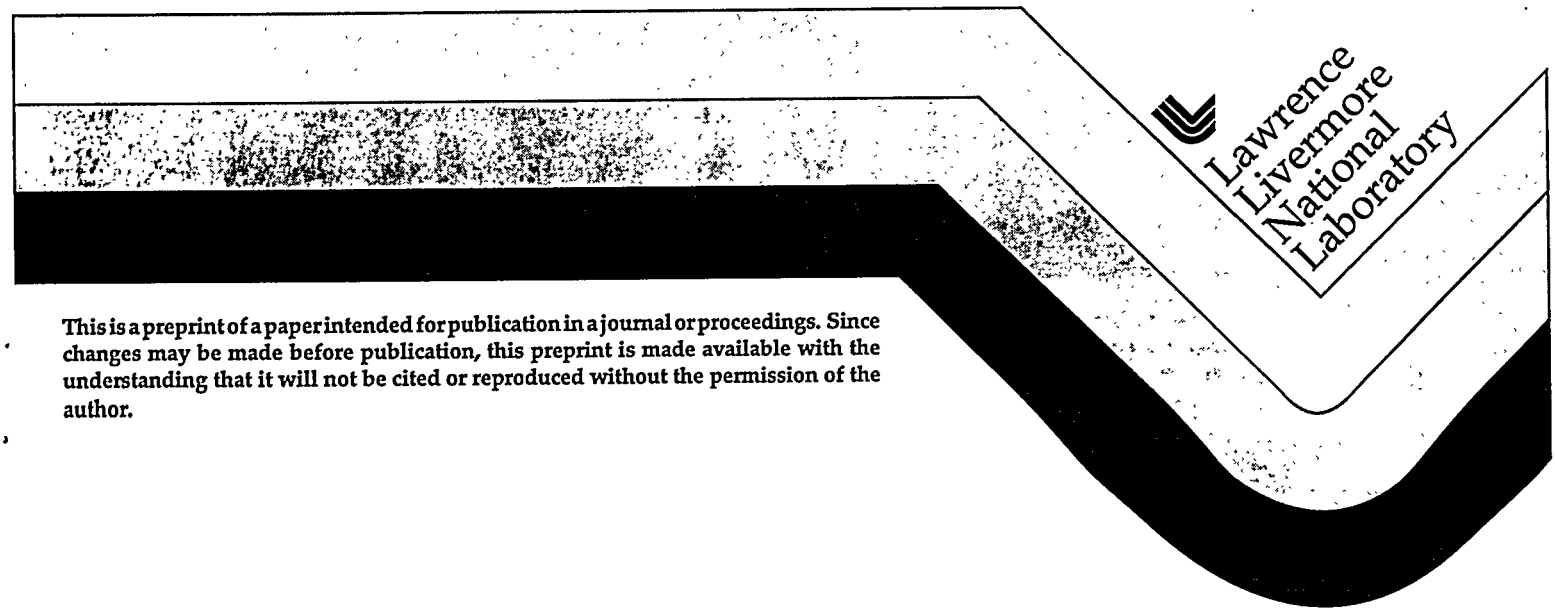

DISCLAIMER

Portions of this document may be illegible in electronic image products. Images are produced from the best available original document.

Plasma electrode pockels cell for ICF lasers

Mark A. Rhodes, Charles D. Boley, Alfonso G. Tarditi, and Bruno S. Bauer

University of California
Lawrence Livermore National Laboratory
Livermore, CA 94550 USA

ABSTRACT

In a plasma-electrode Pockels cell (PEPC), plasma discharges serve as transparent electrodes on each side of an electro-optic crystal such as KDP. These plasmas facilitate rapid and uniform charging and discharging of the crystal. We describe PEPC technology deployed on Beamlet and envisioned for the National Ignition Facility. Performance on Beamlet is discussed in detail. We also discuss models which have shed light on PEPC operation. These models describe both the high-voltage sheath that forms near the crystal surface and the characteristics of the bulk plasma column.

1 INTRODUCTION

Plasma-electrode Pockels cells are an enabling technology for high-energy multipass laser amplifiers.[1] When used in conjunction with a suitable polarizer, they allow, for the first time, active switching of the large-aperture laser beams required for inertial confinement fusion. The PEPC concept was invented at Lawrence Livermore National Laboratory in the middle of the last decade.[2]

In 1991 an intense development was initiated for PEPC technology in the Beamlet laser. This is the first high-energy laser to make use of a PEPC based optical switch. In the Beamlet laser, a PEPC containing a $37 \times 37 \times 1$ cm^3 KDP crystal works in conjunction with a Brewster angle polarizer to form an active optical switch. Figure 1 shows the Beamlet laser with a detail of the optical switch. This PEPC routinely controls multipass amplification in the amplifier cavity, switching optical pulses up to 6 kJ and 3 ns with a switching efficiency of 99.6%.

Day-to-day experiments are also performed on a smaller "prototype" PEPC, which was constructed to validate the Beamlet design and which has a $32 \times 32 \times 1$ cm^3 KDP crystal.

In the next section, we review the operating principles of a PEPC. In Section 3, we review the performance of the Beamlet PEPC. Sections 4 and 5 are devoted to discussions of models. We first consider how the plasma next to the crystal reacts when the switching voltage is applied. This analysis predicts the minimum plasma density required for PEPC operation. We then present a fluid model of plasma formation in a PEPC. This shows how the plasma edge density scales with operating pressure, plasma current, and cell dimensions. The final section contains some concluding remarks.

2 PEPC OPERATING PRINCIPLES

Figure 2 shows a top view of a PEPC along with a schematic of the required external circuit. The PEPC is comprised of two vacuum regions on either side of a KDP crystal. Two fused silica windows seal the outside of the vacuum regions. The vacuum is maintained by a turbo-molecular pumping system. The typical base pressure (no working gas) is 5×10^{-5} torr. The working gas is primarily helium with 1% oxygen. The purpose of the oxygen is described below. The typical operating pressure is 35 mtorr.

On each side of the crystal is a pair of electrodes for discharge formation. For the cathode, we use a planar magnetron structure. The magnetron field is formed by permanent magnets attached to a steel back plate. The magnets and back plate are enclosed by a graphite cover. This type of cathode emits electrons by secondary emission due to bombarding plasma ions. Sputtering of the cathode surface is an unwanted but inevitable byproduct. Since the cathode surface is graphite, the sputtered material is carbon. The oxygen component of the plasma reacts with the carbon to form carbon monoxide and carbon dioxide, which are pumped away and do not deposit on the interior optical surfaces. The anodes are simply bars of stainless steel.

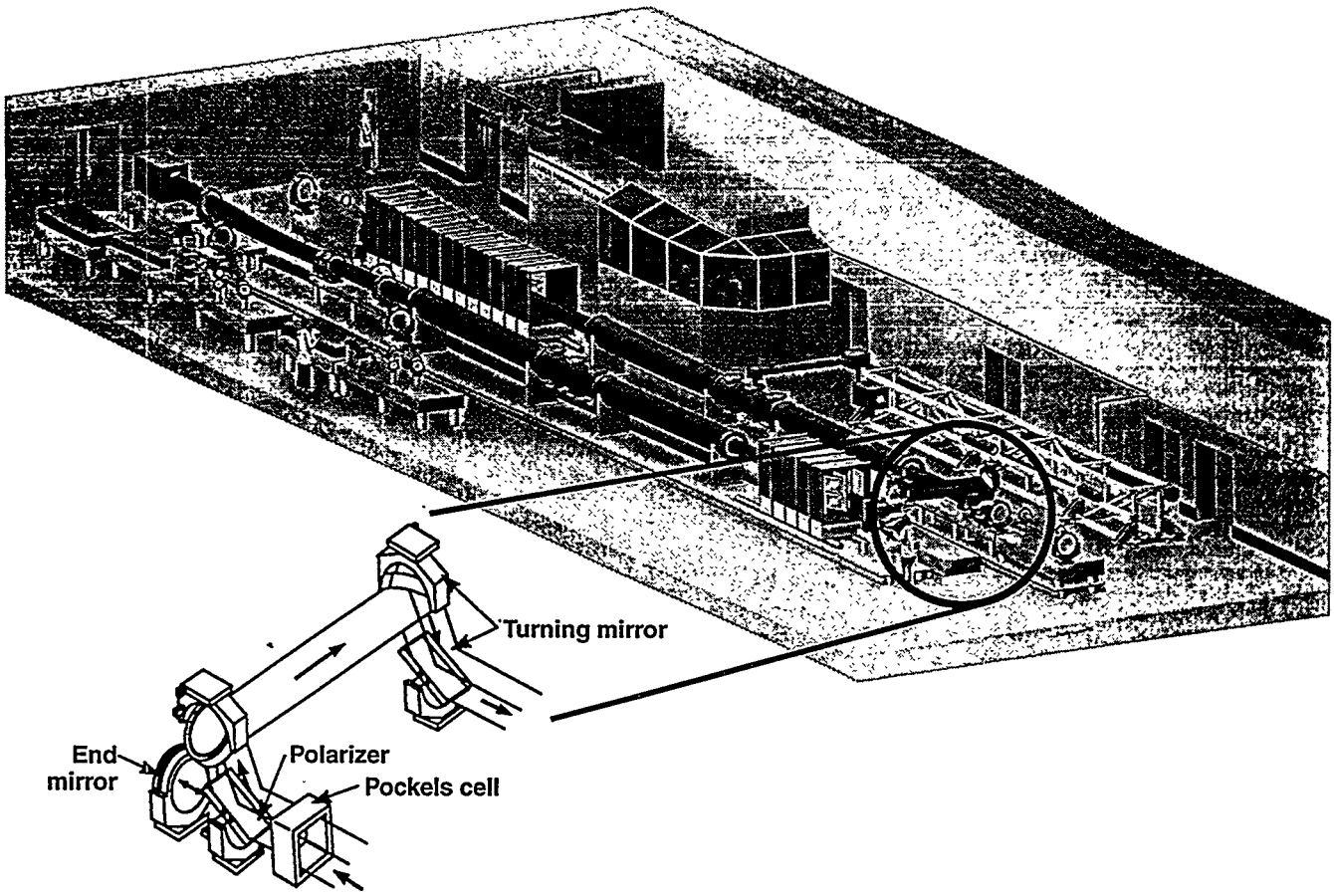

02-30-0392-0431pb01

Figure 1. Beamlet laser, showing detail of the optical switch.

The plasmas are formed by driving a current between the anode-cathode electrode pairs through the working gas. This current is driven by the plasma pulse generators. The plasma is formed in a two step process. Initially we form a low current (40 mA) glow discharge. The operating voltage is about 300 V. We then drive a high-current discharge (2–5 kA) to produce the moderate-density plasma (10^{12} cm^{-3} < n_e < 10^{13} cm^{-3}) required for efficient PEPC operation. Near the current peak of this discharge, we fire the switch pulse generator which charges the KDP crystal to V_π (16.4 kV for KDP). The crystal represents an essentially capacitive load (2500 pF in Beamlet), and the switch pulse impedance must be less than 10 ohms for the PEPC to change state in 100 ns (four *RC* time constants).

3 BEAMLET PEPC PERFORMANCE

The Beamlet laser employs a PEPC to control multipass amplification of an injected optical pulse. Figure 3 shows the Beamlet PEPC as installed in the Beamlet facility. This PEPC uses a 37 cm × 37 cm × 1 cm KDP crystal as the electro-optic element. The PEPC and its associated polarizer are arranged so that with zero voltage applied, the polarization of an incoming optical pulse is unchanged and the amplifier cavity is open. When V_π is applied, the polarization of an incoming beam is rotated by 90 degrees and the cavity is closed. Figure 4 shows typical plasma current and switch-pulse voltage waveforms. Also shown is the timing for the switch voltage and for the three passes which the optical pulse makes through the PEPC in normal Beamlet operation. We arrange the voltage pulse timing so that the optical pulse is trapped in the cavity for four gain passes. Between passes three and four, the PEPC goes from voltage on to voltage off in less than 200 ns.

We evaluate PEPC performance by viewing the transmitted light with the PEPC between a pair of polarizers. The crystal plane is imaged on a high-resolution CCD camera. We process the image data to read in percent switching efficiency. For

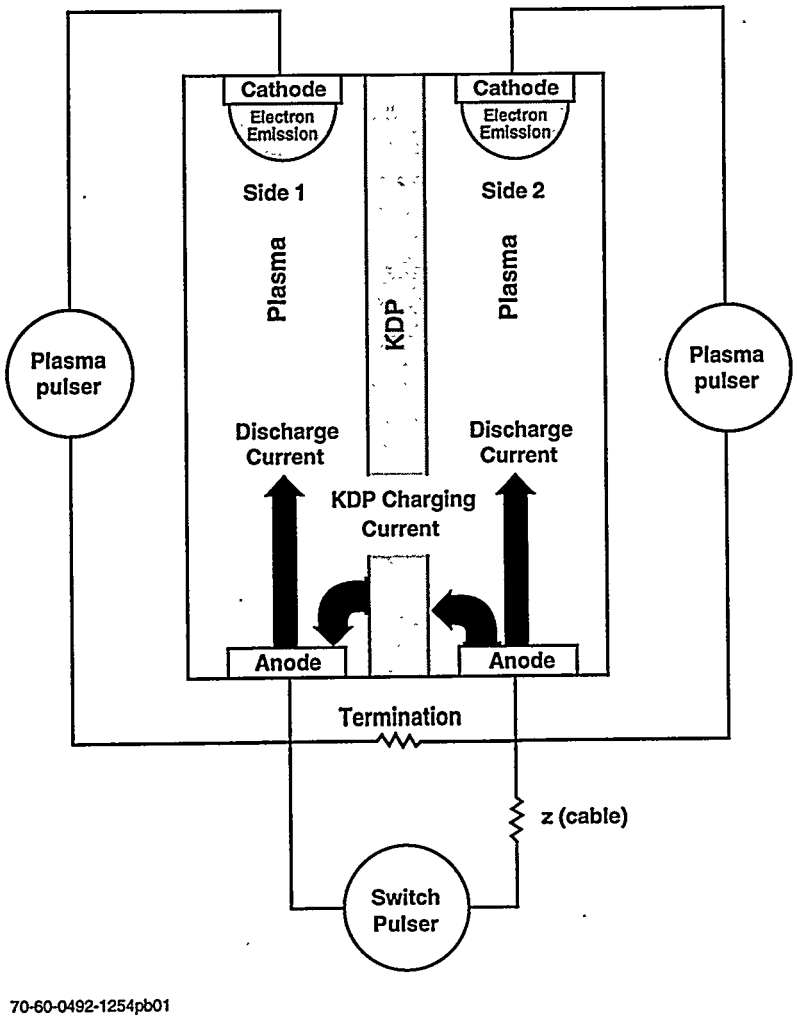

Figure 2. Schematic top view of a PEPC and external circuit.

example, 99% switching efficiency means that only 1% of the light is not switched into the proper polarization by the PEPC-polarizer combination. Switching efficiency does not include losses from surface reflection or absorption in the windows or KDP crystal. Figure 5 shows some typical results. Figure 5(a) shows the static depolarization introduced by the PEPC when not in operation and when not under vacuum, while Figure 5(b) shows the PEPC in full operation. The average switching efficiency across the full aperture is greater than 99.5% for both voltage on and voltage off states. The regions of higher depolarization evident in the four corners are due primarily to strain induced depolarization from the vacuum loading of the fused silica windows.

4 ION LAYER MODEL

When the switch pulse voltage is applied, electrons are pulled toward the crystal on the negative side and away from the crystal on the positive side. An ion layer will open up on the positive side, leading to a voltage drop which opposes the applied voltage. This effect is most pronounced at low plasma edge densities. If the density is too low, the sheath voltage can grow to several kV and still be in the neighborhood of several hundred volts after 200 ns. The maximum width can be several mm. Eventually the sheath collapses to a thermal sheath characterized by a voltage of a few times the electron temperature (thus about 20 volts) and a width of several microns.

The general effect is illustrated in Figure 6, which shows the result of modeling with PDP1, a 1D particle-in-cell (PIC) code.[3] The simulation domain is a 5-mm plasma slab with the x-axis perpendicular to the crystal. An external potential is applied between the right boundary, considered as zero potential, and the crystal. An *RC* series external circuit with the

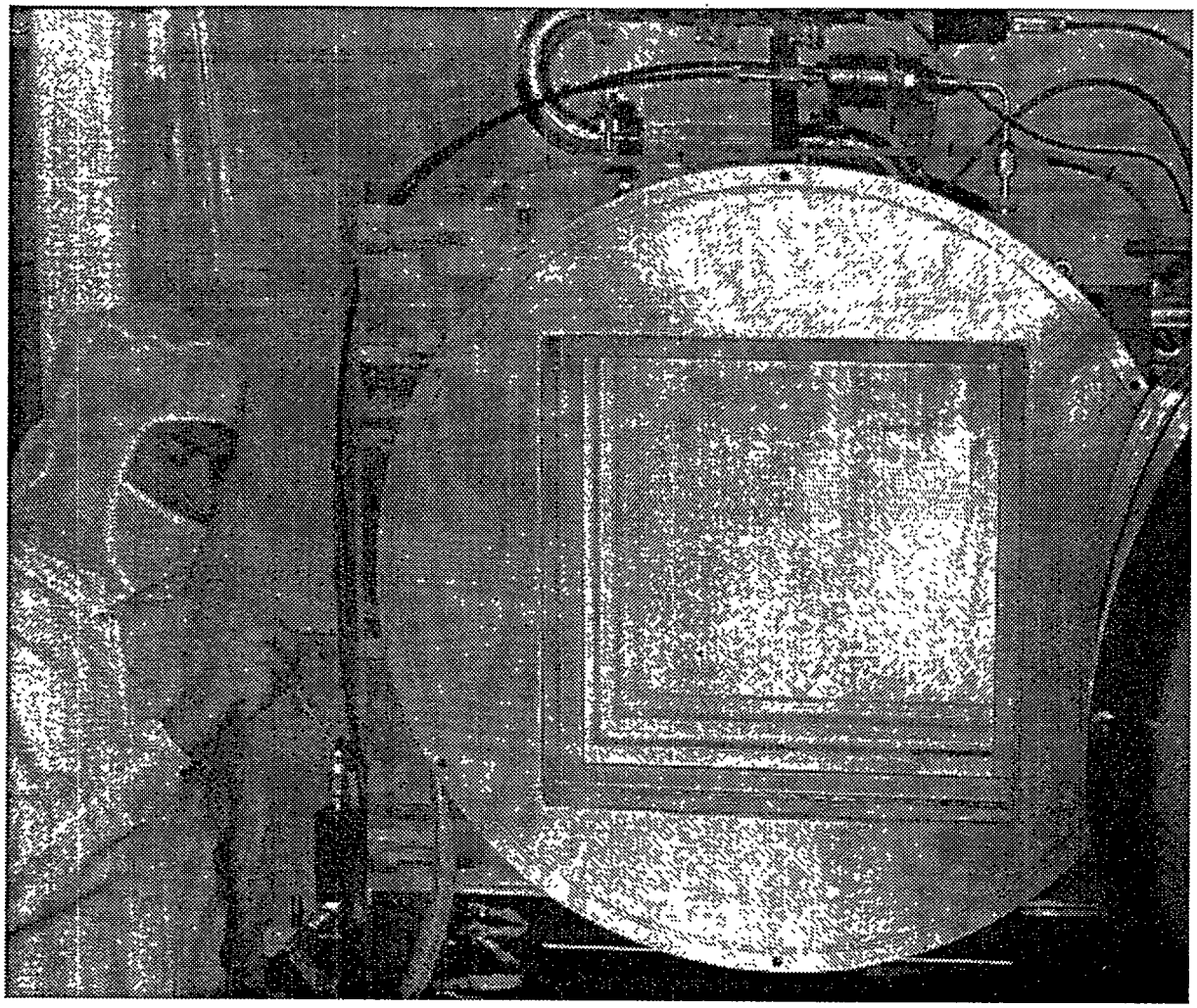

70-50-0894-3237pb01

Figure 3. Beamlet PEPC as installed in Beamlet facility.

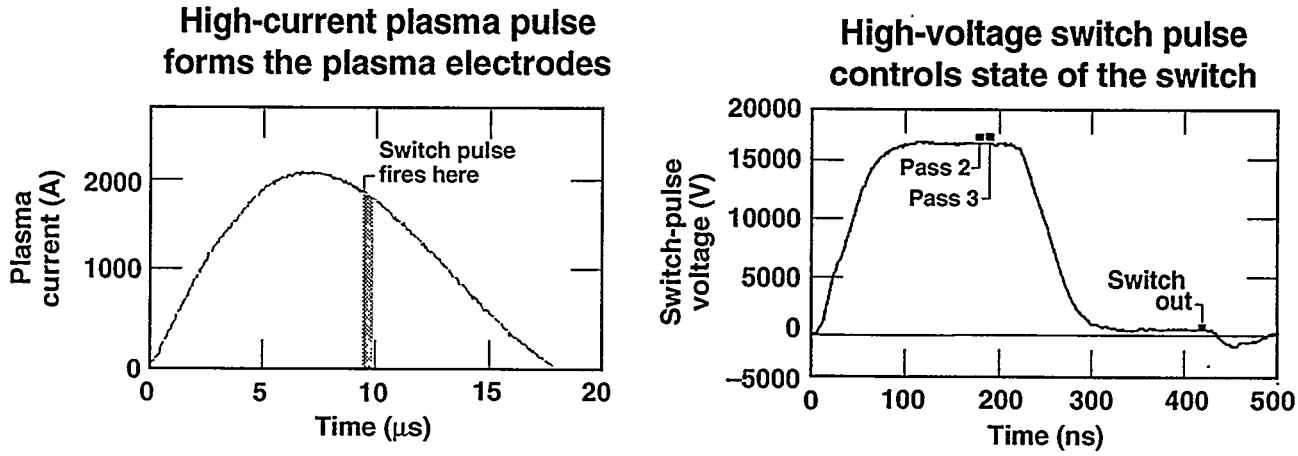

70-50-0494-1849pb01

Figure 4. Typical plasma current and switch-pulse voltage waveforms for the Beamlet PEPC, along with timings. (Note the difference in time scales.)

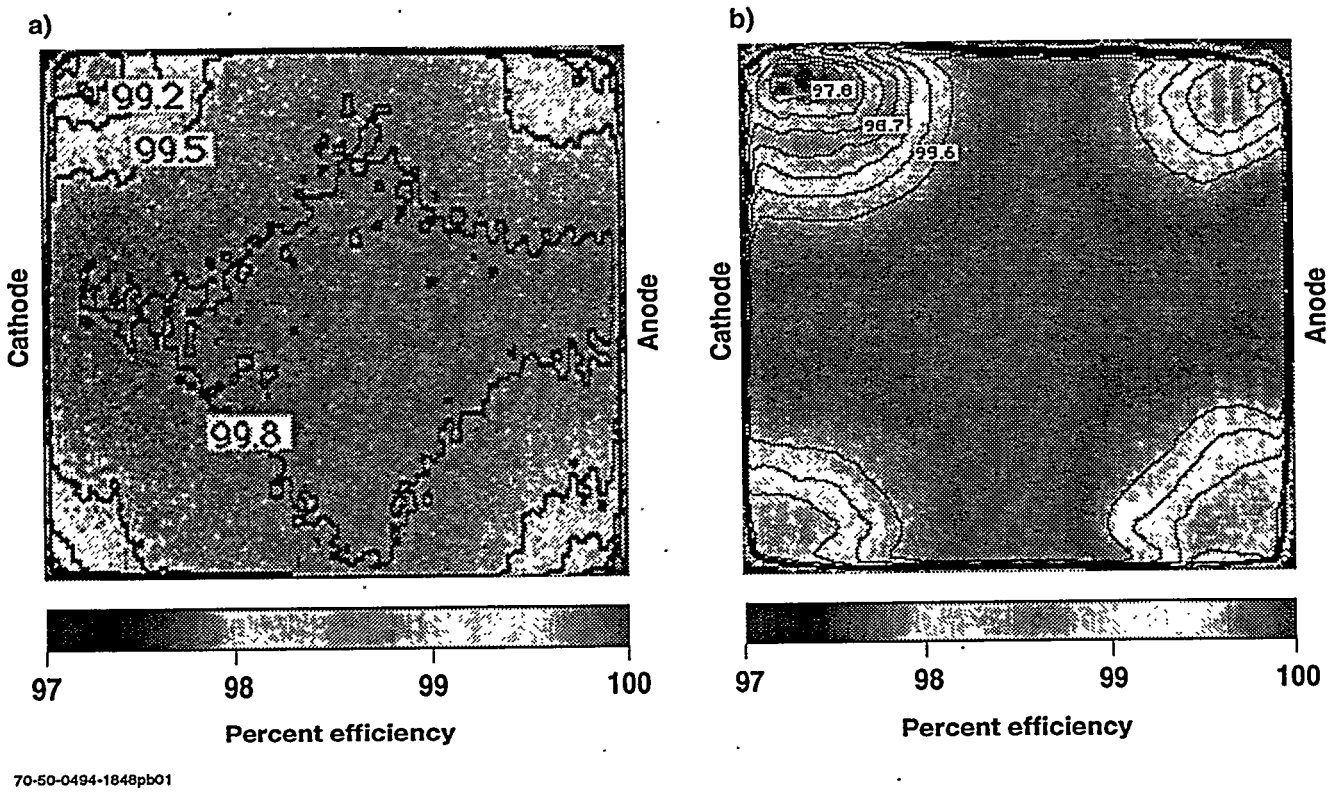

Figure 5. Static depolarization introduced by Beamlet PEPC: (a) when not in operation; (b) when in operation.

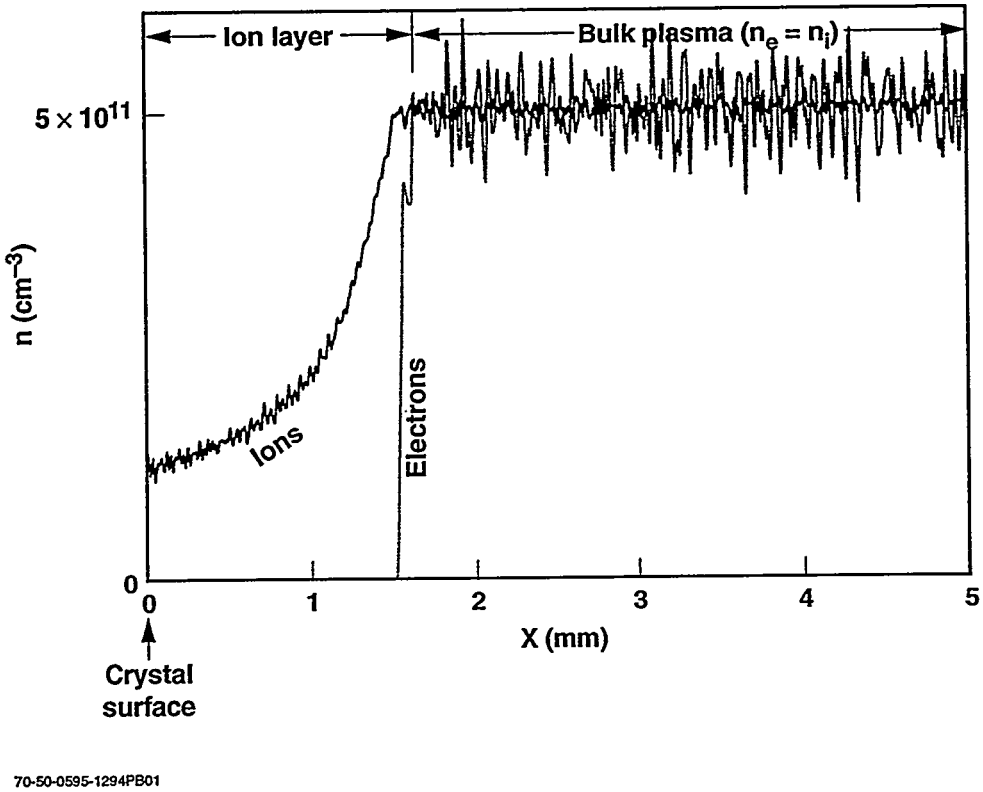

Figure 6. Ion layer as modeled by PDP1. The crystal is on the left.

voltage generator is also included. A uniform plasma is loaded as the initial condition; electrons and ions have a Maxwellian distribution with different temperatures.

When the external potential of 18 kV (negative with respect to the wall) is applied, a current is observed in the plasma. The current rapidly reaches its peak value V_{ext}/R (the limit imposed by the external resistor) and then decays because the sheath potential starts to build up, reducing the electron flow through the plasma. The electron density near the wall eventually drops to virtually zero, while the ion density decreases to a nonzero value. An ion layer is formed between the wall and the quasineutral plasma region. The boundary plates collect the particles that leave the domain. They build up a surface charge density that is used, along with the external circuit equation, in solving for the electrostatic potential.

We have also developed a relatively simple analytic model of this phenomenon. We assume that the layer decays via the ion saturation current, which is taken to be proportional to the edge ion density (also equal to the edge electron density) and the Bohm speed, i.e. $I_s = en_e v_B A$, with $v_B = (T_e/M_i)^{1/2}$, A the area of the crystal, and M_i the ion mass (the electron temperature T_e is measured in energy units). On the time and spatial scales of interest, we treat n_e as a fixed parameter. Thus the charge in the sheath satisfies $\dot{Q}_s = I - en_e v_B A$, where I is the total switch-pulse current. We have employed a "matrix" sheath model, in which the ion density across the sheath is uniform and the electron density vanishes.[4] We require only the relation between the charge Q_s in the sheath and the voltage V_s across it. For the matrix sheath, this is $V_s = Q_s^2/2\varepsilon_0 en_e A^2$.

Figure 7 shows the calculated sheath and crystal voltages, as functions of time, for two choices of plasma edge density. From the fluid model of the next section, we take $T_e = 5$ eV. Note that PDP1 and the analytic model give qualitatively similar results, although the voltage predicted by the latter is systematically higher by at least 2 kV. For a low edge density ($n_e = 5 \times 10^{11}$ cm^{-3}), the sheath opens up to 7–9 kV, depending on the model, and has not fully decayed even after 200 ns (in the analytic model). At twice this edge density, on the other hand, the sheath reaches only about half this maximum voltage and has disappeared after 200 ns.

The edge density serves as an input parameter to the analytic model. We can estimate it by comparing predicted current waveforms with measurements taken on the prototype PEPC. For this purpose, we turn first to the case of a high (maximum 2

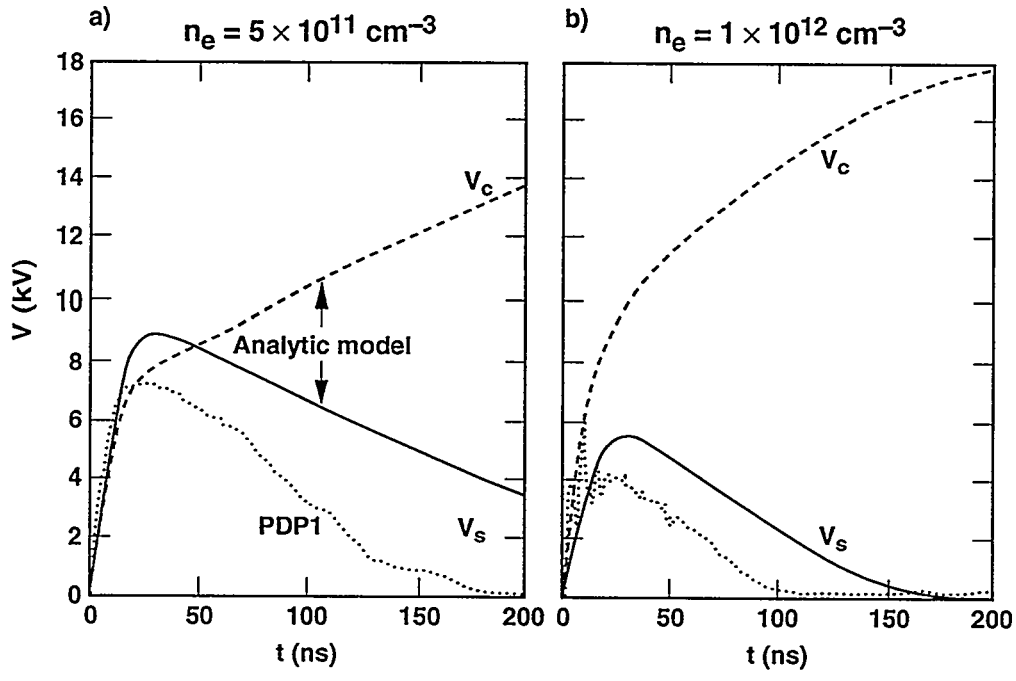

Figure 7. Calculated voltages across the ion layer sheath and the crystal, as functions of time: (a) low edge electron density; (b) high edge density.

kA) plasma current. The experimental current, shown in Figure 8(a), has fully decayed after 100 ns, suggesting that the edge density is sufficiently high to overcome the ion layer effect. For the model to match this, an input edge density of at least 6.3×10^{12} cm^{-3} is required. At this edge density, and at higher values, the calculated sheath potential is insignificant.

The case of a lower peak plasma current (maximum 500 A) is shown in Figure 8(b). Here the data indicate not only long-time current flow but also current clamping. We interpret the former as the ion saturation current and the latter as an indication that the anode on the negative-side plasma cannot turn negative and begin acting as a cathode. Thus the charging current cannot exceed the sum of the plasma current and the ion saturation current to this anode. We incorporate this condition in the model, taking the anode ion saturation current from experiment. Such a condition has no effect in the previous case. Applying the model, we find best agreement for an edge density of 1.6×10^{12} cm^{-3}, or about a quarter of the minimum edge density inferred for the previous case. It is encouraging that the model does a reasonable job of reproducing experiment over the entire time range.

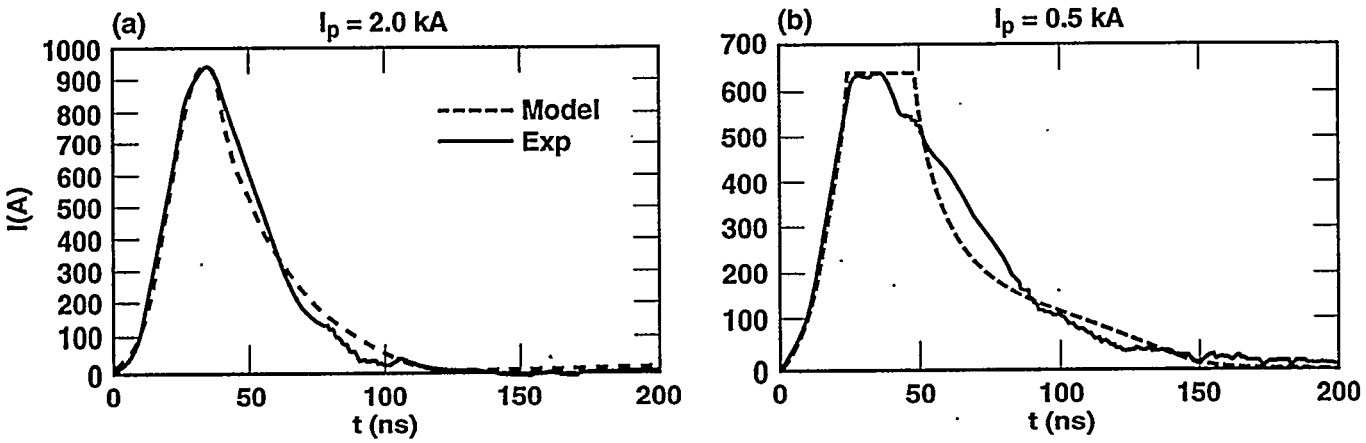

Figure 8. Switch current waveforms for (a) high plasma current and (b) low plasma current, and modeling results.

5 FLUID MODEL

Elementary considerations show that, sufficiently far from the electrodes, a quasineutral positive column extends across the crystal.[4] The plasma parameters within the column are independent of the distance along the column. They are determined instead by the fluid continuity equations with spatial variation in the short direction, i.e. perpendicular to the crystal. (We assume that the current is uniform in the vertical direction.) We now evaluate the plasma parameters, assuming for simplicity that the driving current changes little over characteristic plasma time scales, so that equilibrium conditions exist. The characteristic times (for ionization, momentum transfer, and ambipolar diffusion) all lie in the neighborhood of a few microseconds.

The continuity equation for the electron density has the form

$$\frac{\partial(n_e v_x)}{\partial x} = n_e n_0 \kappa_{ioniz}, \tag{1}$$

where n_e is the electron density (equal to the ion density because the column is quasineutral), v_x is the common velocity of electrons and ions, $\kappa_{ioniz}(T_e)$ is the rate coefficient for ionization, and x is the distance in the direction perpendicular to the crystal. The depletion of the neutral density n_0 via ionization, an effect on the order of a percent, is neglected. The electron and ion velocity equations are

$$m_e n_e v_x \frac{\partial v_x}{\partial x} = -e n_e E - \frac{\partial n_e}{\partial x} T_e - m_e n_e n_0 \kappa_{e0} v_x, \tag{2}$$

$$M_i n_e v_x \frac{\partial v_x}{\partial x} = e n_e E - M_i n_e n_0 \kappa_{cx} v_x, \tag{3}$$

in which we have ignored the ion temperature. The quantities κ_{e0} (T_e) and κ_{cx} are rate coefficients for electron-neutral momentum transfer and charge exchange. Since this region of the plasma is quasineutral, the electric field serves to make the electron and ion velocity equations consistent but does not satisfy Poisson's equation. In practice, we add the electron and ion velocity equations and solve for the electric field at the end of the calculation. If the inertial terms (those involving $\partial v_x/\partial x$) were omitted in the velocity equations, we would have the ambipolar diffusion approximation with $D = T_e/n_0 (M_i \kappa_{cx} + m_e \kappa_{e0})$. The inertial terms allow the model to hold nearly to the edge of the sheath.[5]

Because of the high electron thermal conductivity, the electron temperature can be taken as uniform. The power balance is then given by

$$\rho J^2 = n_e T_e \frac{\partial v_x}{\partial x} + n_e n_0 \left[(E_{ion} + 3T_e/2) \kappa_{ioniz} + E_{rad} \kappa_{rad} \right] + \frac{3m_e}{M_i} n_e n_0 \kappa_{e0} T_e, \tag{4}$$

where the plasma resistivity is $\rho = m_e n_0 \kappa_{e0}/n_e e^2$. The left-hand side is the ohmic heating input, while the right-hand side represents losses due to convection, ionization, radiation, and temperature equilibration, respectively.

The density and velocity equations decouple from the energy equation. Solving for the derivatives, we see that the discriminant vanishes at $v_x = v_B$. The velocity begins at zero at the center ($x = 0$) and then increases until the point at which it reaches the Bohm speed, where its gradient becomes infinite. The equations cannot be continued beyond this point x_{max}, which we interpret as the beginning of the sheath. Physically, this behavior comes about because effects due to charge separation become important. The plasma width $w = 2x_{max}$ satisfies

$$(\nu_0/v_B) x_{max} = (\alpha + 1/\alpha) \tan^{-1}(1/\alpha) - 1, \tag{5}$$

where ν_0 is the effective momentum transfer frequency and α is the ratio of the ionization frequency to this frequency:

$$\nu_0(T_e) = n_0 \left[\kappa_{cx} + (m_e/M_i) \kappa_{e0} \right], \quad \alpha(T_e) = \left(n_0 \kappa_{ioniz}/\nu_0 \right)^{1/2}. \tag{6}$$

Equation (5) gives the product of the pressure and the width as a function of electron temperature. Inverting it, we obtain $T_e = T_e(pw)$ as illustrated in Figure 9(a). The electron temperature varies inversely with pw, since diffusion effects decrease with increasing pressure and/or width, thus requiring a lower level of ionization. For the prototype PEPC, T_e is about 5 eV, while for the Beamlet PEPC it is about an electron volt lower. Similarly, the ratio of the edge density to the central density can be expressed as a function of the product of pressure and width. The result is shown in Figure 9(b). The density ratio decreases with the pressure-width product for the same reason as for the electron temperature. The ratio is about 0.25 for the prototype PEPC, while it is 40% lower for the Beamlet PEPC.

To obtain the absolute level of the plasma density, we turn to the power balance, as given in Eq. 4. Solving for the current density and integrating over the width, we can express the average current density as a product of the edge density and a complicated function of T_e. The edge density can then be written in the form

$$n_e(x_{max}) = C \frac{I}{hw} g(pw), \tag{7}$$

with h the plasma height and $C = 10^{12}$ (kA cm)$^{-1}$. The dimensionless function $g(pw)$ is numerically close to 200 for cases of interest. Sample curves are given in Figure 10. Note that the edge density is directly proportional to the average current density. This explains why the Beamlet PEPC requires more current than the thinner prototype in order to reach about the same edge density. The specific edge densities predicted at currents of 2 kA and 0.5 kA are about a factor of four lower than those estimated in the previous section via the ion layer model. One explanation of this difference might be that current pinching occurs, leading to an enhanced current density and thus to an increased edge density. The improvement might also be increased by extension of the ion layer model to a full 1D description.

Finally, we turn to the effect of time dependence on these results. The concern here is that typical plasma response times are a few microseconds, while the plasma current rises from near zero to peak in some 7 microseconds. Inserting time derivatives into the fluid equations, we have obtained solutions via the method of lines. We now consider the effects of

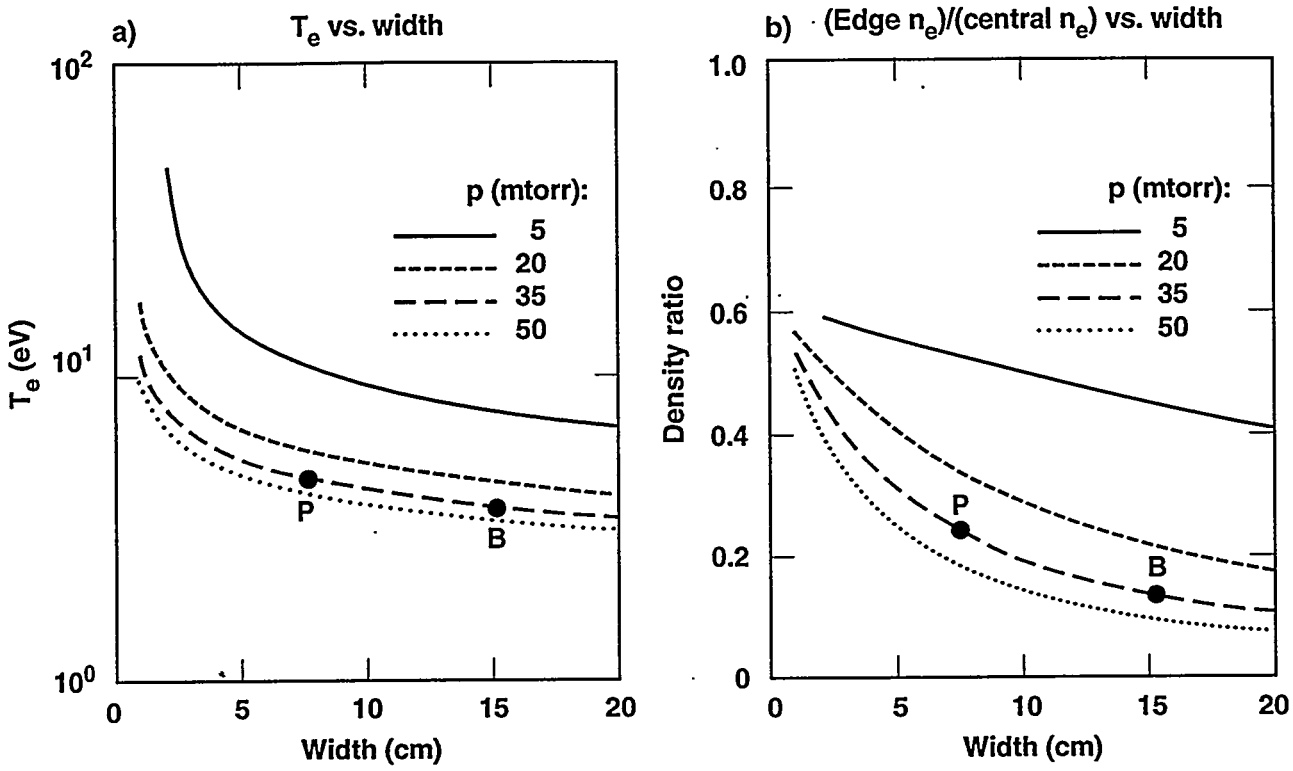

1.1.2.0295.0436pb01

Figure 9. Predictions of the fluid model: (a)electron temperature versus cell width; (b) edge electron density (normalized by central electron density) versus width. Points P and B refer to the prototype PEPC and Beamlet PEPC, respectively.

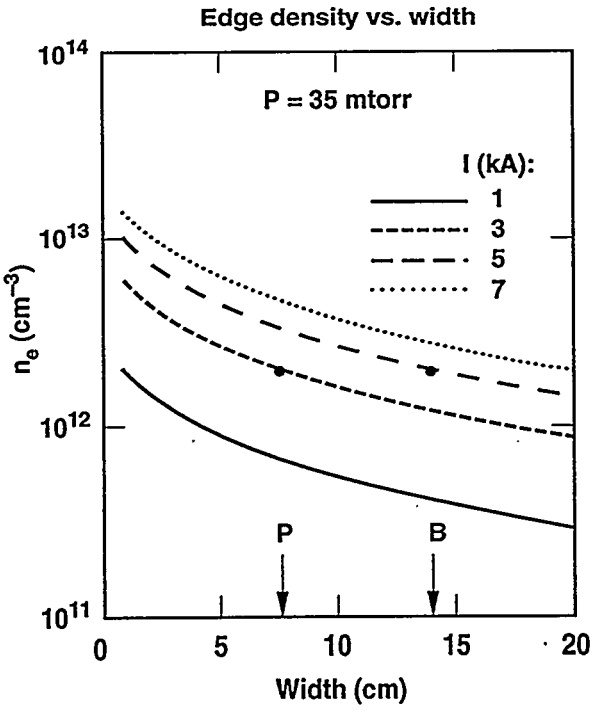

1.1.2.0295.0438pb02

Figure 10. Fluid model predictions for edge electron density versus cell width.

varying the current pulse length from 1 to 50 microseconds, with a fixed peak value of 3 kA. Figure 11 shows the resulting maximum edge density for PEPCs of three widths: the one on Beamlet, the prototype, and one of half the prototype width (envisioned for NIF). In each case the edge density approaches its equilibrium value as the pulse is lengthened. Higher density is achieved at shorter pulse lengths with the thinner cells. The reason is that ambipolar diffusion is most rapid for small widths. The NIF design has a relatively thin cell (3.75 cm) in order to take advantage of this effect. Current instabilities are expected to place a lower bound on the cell width.

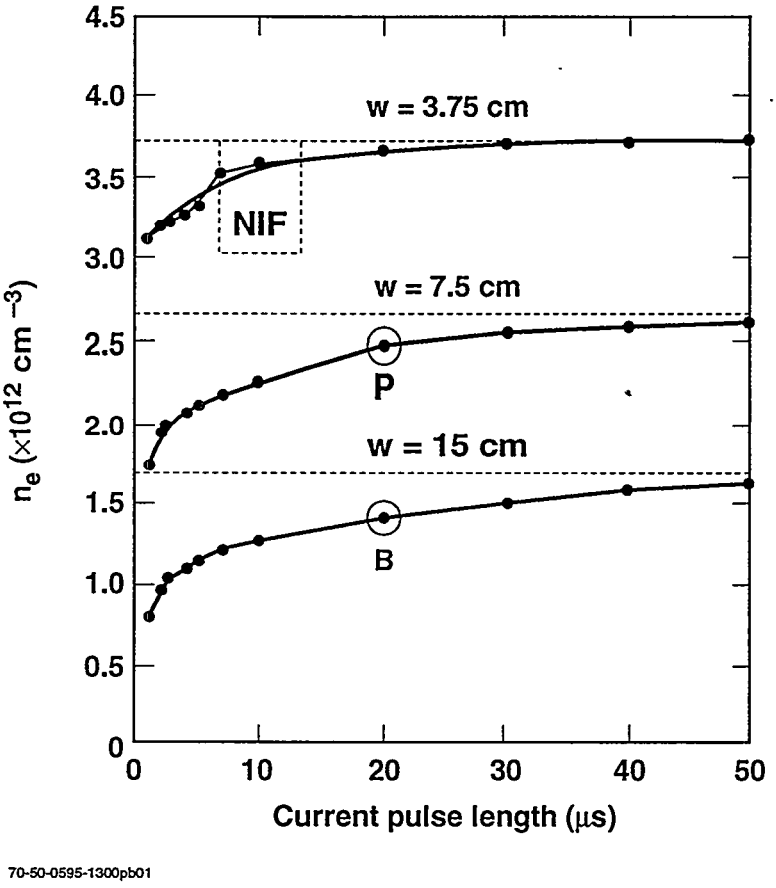

Figure 11. Maximum edge density as a function of switch pulse length, for cells of three widths.

6 CONCLUSIONS

In this paper, we have described the principles and operation of a plasma-electrode Pockels cell. The focus of our effort has been a PEPC for the Beamlet laser, which was built to demonstrate new technologies for ICF. The Beamlet PEPC routinely switches a 6 kJ, 3 ns optical pulse with an efficiency greater than 99.5%. We have described how the PEPC is configured and how it operates. We have presented a model of the crystal charging process which shows that formation of an ion layer can inhibit complete charging of the KDP crystal if the plasma density is too low. This model predicts the minimum density required for PEPC operation. We have also described a fluid model of the plasma formation. This model predicts the plasma edge density as a function of operating pressure, cell dimensions, and plasma current. It indicates that there are two advantages to decreasing the width of the cell: the plasma edge density should increase (for a given plasma current), and the current pulse duration can be shortened. Experimental and modeling results are being used to optimize the design of a multi-aperture PEPC required for the planned National Ignition Facility.

*Work performed under the auspices of the U.S. Department of Energy by Lawrence Livermore National Laboratory under Contract No. W-7405-Eng-48.

REFERENCES

1. M. A. Rhodes, B. Woods, J. J. DeYoreo, D. Roberts, and L. J. Atherton, "Performance of Large-Aperture Optical Switches for High-Energy ICF Lasers," Applied Optics (1995).

2. J. Goldhar and M. A. Henesian, "Large-Aperture Electrooptical Switches with Plasma Electrodes," IEEE J. Quantum Electronics **QE-22**, 1137-1147 (1986).

3. V. Vahedi, J. P. Verboncoeur, and C. K. Birdsall, "XPDP1, Plasma Device 1 Dimensional Bounded Electrostatic Code," University of California, 1992.

4. See, e.g., M. A. Lieberman and A. J. Lichtenberg, "Principles of Plasma Discharges and Materials Processing," John Wiley and Sons, Inc., 1994.

5. K.-U. Riemann, "The Bohm Criterion and Sheath Formation," J. Phys. D **24**, 493 (1991).